

BANDGAP ENGINEERING OF CARBON ALLOTROPES

Vijay K. Arora

Faculty of Electrical Engineering, Universiti Teknologi Malaysia, UTM Skudai 81310
Department of Electrical Engineering and Physics, Wilkes University, Wilkes-Barre, PA
18766, U. S. A.

Abstract. *Starting from the graphene layer, the bandgap engineering of carbon nanotubes (CNTs) and graphene nanoribbons (GNRs) is described by applying an appropriate boundary condition. Linear E-k relationship of graphene transforms to a parabolic one as momentum vector in the tube direction is reduced to dimensions smaller than inverse of the tube diameter of a CNT. Similar transition is noticeable for narrow width of a GNR. In this regime, effective mass and bandgap expressions are obtained. A CNT or GNR displays a distinctly 1D character suitable for applications in quantum transport.*

Key words: *bandgap engineering, graphene, carbon nanotube, graphene nanoribbon, NEADF, carrier statistics*

1. INTRODUCTION

Carbon allotropes have their basis in graphene, a single layer of graphite with carbon atoms arranged in a honeycomb lattice. Graphene has many extraordinary electrical, mechanical, and thermal properties, such as high carrier mobility, ambipolar electrical field effect, tunable band gap, room temperature quantum Hall effect, high elasticity, and superior thermal conductivity. It is projected to be a material of scientific legend, comparable only to penicillin as a panacea. There is a modern adage: silicon comes from geology and carbon comes from biology. Cohesive band structure of graphene rolled into a CNT in a variety of chiral directions has recently been reported [1]. Graphite, a stack of graphene layers, is found in pencils. As shown in Fig. 1, formation of these allotropes originates from a graphene layer through various cutouts. A carbon nanotubes (CNT) is a rolled-up sheet of graphene (Also see Fig. 2). A fullerene molecule is a “buckyball,” nanometer-size sphere. A graphene nanoribbon (GNR) is a cutout from a graphene sheet with a narrow width of high aspect ratio.

Received January 10, 2014

Corresponding author: Vijay K. Arora

Wilkes University, E-Mail: vijay.arora@wilkes.edu

(e-mail: vijay.arora@wilkes.edu)

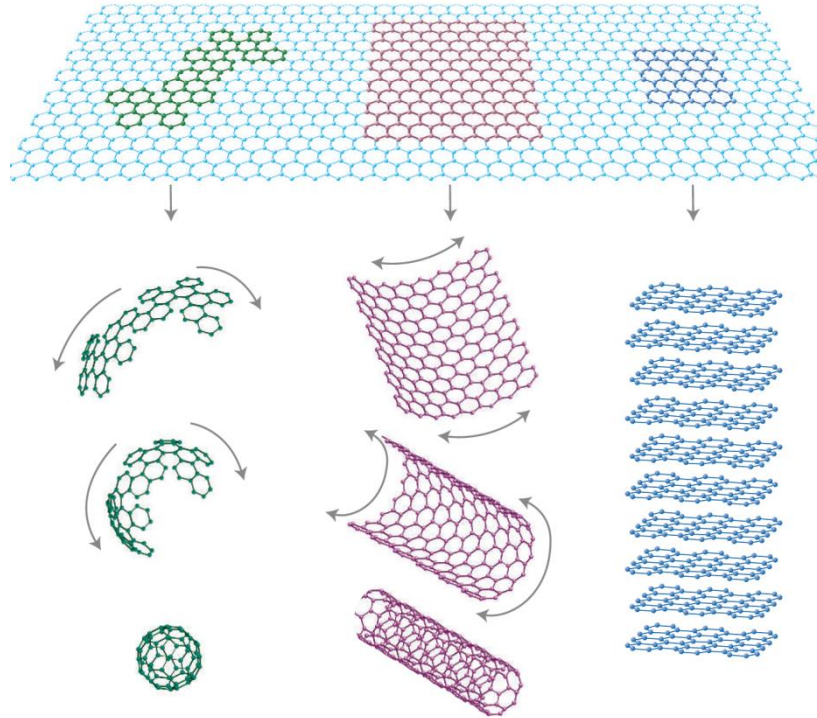


Fig. 1 Carbon allotropes arising from graphene sheet to form zero-dimensional (0D) buckyball, one-dimensional (1D) CNT, and three dimensional graphite (3D). Each layer of two-dimensional (2D) graphite can be converted to a 1D GNR by making width smaller. Copyright Macmillan Publishers Limited [2], A. K. Geim and K. S. Novoselov, "The rise of graphene," *Nature Materials*, vol. 6, pp. 183-191, Mar 2007

Carbon (${}_6\text{C}^{12}$) atom with 6 electrons has electronic configuration $1s^2 2s^2 2p^2$. It is a tetravalent material with four of its electrons in shell 2 and still able to accommodate 4 more in 2p orbitals. However, carbon orbitals can hybridize because the s-orbital and p-orbitals of carbon's second electronic shell have very similar energies [3]. As a result, carbon can adapt to form chemical bonds with different geometries. Three sp^2 orbitals form σ -bond residing in the graphene plane of Fig. 2. These are pretty strong bonds that demonstrate superior electronic properties. Fourth electron with π -bond is delocalized conduction electron. Each atom contributes $1/3^{\text{rd}}$ of the π -electron to a hexagon. With 6 atoms forming corners of a hexagon, each hexagon contributes 2 π -electrons. The areal electronic density of π -electrons is $n_g = 2/A_h$ with $A_h = 3\sqrt{3}a_{cc}^2/2$ is the area of the hexagon. The areal density is $n_g = 3.82 \times 10^{19} m^{-2}$ with C-C bond length of $a_{cc} = 0.142 nm$. The intrinsic line density in a CNT is expected to be a function of diameter $n_{CNT} = 1.2 \times 10^{11} d_t (nm) m^{-1}$ when rolled into a CNT. Similarly, the line density of GNR is expected to be $n_{GNR} = 3.82 \times 10^{10} W (nm) m^{-1}$.

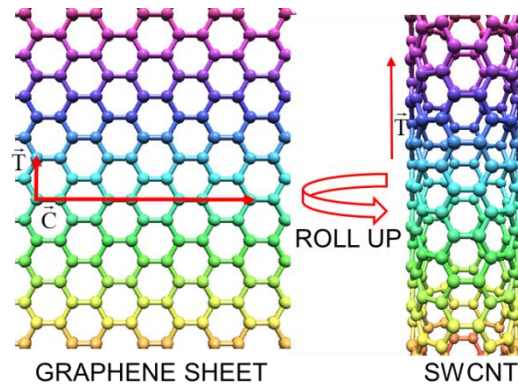


Fig. 2 The rolled up graphene sheet into a carbon nanotube

In recent years, there is a transformation in the way quantum and ballistic transport is described [3]. Equilibrium carrier statistics with large number of stochastic carriers is the basis of any transport. Nonequilibrium Arora's distribution function (NEADF) [4] seamlessly transforms the stochastic carrier motion in equilibrium with no external influence into a streamlined one in a high-field-initiated extreme nonequilibrium for current to flow and get saturated. A new paradigm for characterization and performance evaluation of carbon allotropes is emerging from the application of NEADF to graphene and its allotropes.

2. BANDGAP ENGINEERING

The electronic quantum transport in a carbon nanotube (CNT) is sensitive to the precise arrangement of carbon atoms. There are two families of CNTs: single-wall SWCNT and multiple-wall MWCNT. The diameter of SWCNT spans a range of 0.5 to 5 nm. The lengths can exceed several micrometers and can be as large as a cm. MWCNT is a cluster of multiply nested or concentric SWCNTs. The focus here is on SWCNT. Depending on the chirality, rollup of Fig. 2 can lead to either a semiconducting or metallic state. When the arrangement of carbon atoms is changed by mechanical stretching, a CNT is expected to change from semiconducting to metallic or vice versa. Several unique properties result from the cylindrical shape and the carbon-carbon bonding geometry of a CNT. Wong and Akinwande [3] are vivacious in connecting physics and technology of a graphene nanolayer to that of a CNT with splendid outcomes. CNT band structure arising out of 6-fold Dirac K-points with equivalency of K and K' points can lead to complex mathematics. However, once nearest neighbor tight binding (NNTB) formalism is applied, the resulting Dirac cone, as revealed in Fig. 2, gives useful information for a variety of chirality directions. In fact, the K-points offer much simplicity for quantum transport applications. In the metallic state E-k relation is linear. However, the Fermi energy and associated velocity are different in the semiconducting state. Intrinsic Fermi energy $E_{F_0} = 0$ is applicable for undoped or uninduced carrier concentration. Induction of carriers will move the Fermi level in the conduction (n-type) or valence band (p-type).

Linear E-K relation can be written in terms of k_t , the momentum vector in the longitudinal direction of the tube, and k_c , the momentum vector in the direction of rollup. The new description becomes

$$E = E_{F_0} \pm \hbar v_F |k| = E_{F_0} \pm \hbar v_F \sqrt{k_t^2 + k_c^2} \quad (1)$$

The K-point degeneracy is crucial to the profound understanding of the symmetries of graphene folding into a CNT in a given chiral direction. Symmetry arguments indicate two distinct sets of K points satisfying the relationship $\vec{K} = -\vec{K}'$, confirming the opposite phase with the same energy. There are three K and three K' points, each K (or K') rotated from the other by $2\pi/3$. The zone degeneracy $g_k = 2$ is based on two distinct sets of K and K' points in addition to spin degeneracy $g_s = 2$. There are six equivalent K points, and each K point is shared by three hexagons; hence $g_K = 2$ is for graphene as well as for rolled-up CNT. The phase $k_c C_h$ of the propagating wave $e^{ik_c C_h}$ in the chiral direction results in rolled up CNT to satisfy the boundary condition

$$k_c C_h = \nu(2\pi/3) \quad (2)$$

where $\nu = (n - m) \bmod 3 = 0, 1, 2$ is the band index. $(n - m) \bmod 3$ is an abbreviated form of $(n - m)$ modulo 3 that is the remainder of the Euclidean division of $(n - m)$ by 3. The quantization condition transforms to $k_c = \nu(2/3d_t)$ when $C_h = \pi d_t$ is used for a CNT's circular parameter. Using $k_c = \nu(2/3d_t)$ in Eq. (2) yields the band structure as given by

$$E = E_{F_0} \pm \hbar v_F |k| = E_{F_0} \pm \hbar v_F \sqrt{k_t^2 + \left(\nu \frac{2}{3d_t}\right)^2} \quad (3)$$

The equation is re-written to introduce the bandgap near $k_t \approx 0$

$$E = E_{F_0} \pm \hbar v_F \left(\nu \frac{2}{3d_t}\right) \sqrt{1 + \left(\frac{3d_t k_t}{2\nu}\right)^2} = E_{F_0} \pm \frac{E_g}{2} \sqrt{1 + \left(\frac{3d_t k_t}{2\nu}\right)^2} \quad (4)$$

With the binomial expansion $(1+x)^{1/2} \approx 1 + \frac{1}{2}x$ near the lowest point ($k_t \approx 0$) of the subband and keeping first order term transforms (3) to

$$E = E_{F_0} \pm \left(\frac{E_g}{2} \pm \frac{\hbar^2 k_t^2}{2m_t^*}\right) \quad (5)$$

with

$$E_g = \nu \frac{4}{3d_t} \hbar v_F = \nu \frac{0.88 \text{ eV} \cdot \text{nm}}{d_t} \quad \text{and} \quad \frac{m_t^*}{m_o} = \nu \frac{2}{3d_t} \frac{\hbar}{v_F m_o} = \nu \frac{0.077 \text{ nm}}{d_t} \quad (6)$$

Here $|v_F| = \frac{3a_{cc}\gamma}{2\hbar} = 10^6 \text{ m/s}$ with $\gamma = 3.1 \text{ eV}$ the C-C bond strength.

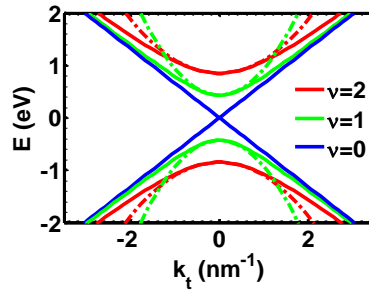


Fig. 3 E_v vs k_t graph with chirality (10,4) for $\nu = 0$, (13,0) for $\nu = 1$, and (10,5) for $\nu = 2$, all with diameter $d_t \approx 1.0 \text{ nm}$. Solid line is used for exact formulation (Eq. 3) and dash-dot line showing parabolic approximation (Eq. 4)

Fig. 3 displays the $E_v - k_t$ relationship for $\nu = 0$ metallic and $\nu = 1(2)$ semiconducting (SC1(2)) states. ν is the band index confined to these three values only as $\nu = 3$ is equivalent to $\nu = 0$ and pattern repeats itself in these three modes. The diameter is $d_t \approx 1.0 \text{ nm}$ for the chosen chirality directions: (10,4) for $\nu = 0$, (13,0) for $\nu = 1$, and (10,5) for $\nu = 2$. Assuming that each of these configurations are equally likely, about $1/3^{\text{rd}}$ of the CNTs are metallic and $2/3$ semiconducting with bandgap that varies with chirality. As seen in Fig. 3, the curvature near $k_t = 0$ is parabolic making it possible to define the effective mass that also depends on chirality. Fig. 4 shows the bandgap of CNTs with different chiral configurations, covering metallic ($\nu = 0$) and two semiconducting ($\nu = 1,2$) states. As expected, the bandgap is zero for metallic state, in agreement with Eq. (4). SC2 bandgap is twice as large as that of SC1. Fig. 4 also shows chirality leading to $\nu = 0, 1$ or 2 . The NNTB bandgap is likewise shown. It also exhibits the wide band gap nature of SC2.

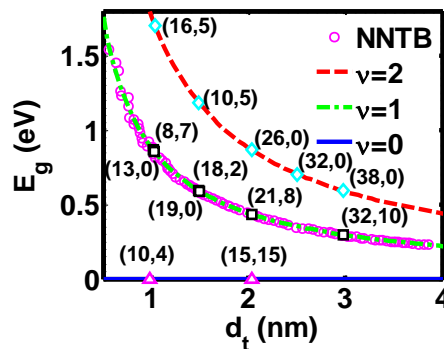


Fig. 4 Calculated band gap as a function of CNT diameter showing an agreement with NNTB calculation. Chiral vectors are indicated against corresponding points

GNR, as shown in Fig. 5, are strips of graphene with ultra-thin width ($<50 \text{ nm}$). The electronic states of GNRs largely depend on the edge structures. The precise values of the bandgaps are sensitive to the passivation of the carbon atoms at the edges of the nanoribbons. Just like for a CNT, bandgap dependence on inverse width is preserved.

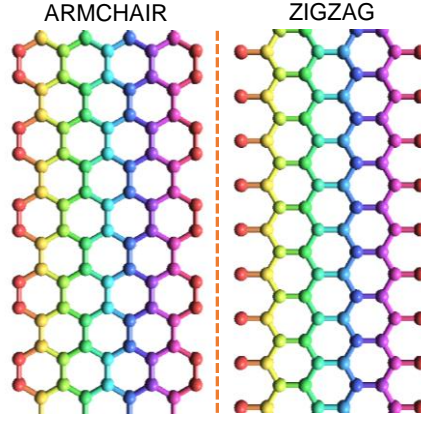


Fig. 5 Armchair and zigzag graphene nanoribbons (GNR) where edges look like armchair and zigzag respectively

In momentum k -space, there are bonding and anti-bonding wavefunctions. In the absence of a magnetic field, forward k and backward $-k$ moving states have identical eigenenergies as is well-known both for parabolic semiconductors as well as for graphene with $E = \hbar v_{F_0} |k|$. This degeneracy occurs both at K and K' with $\vec{K}' = -\vec{K}$. The total phase change as one starts from one of the three K points to other two and returning to the same one is π . The angular spacing between K and K' in k -space is $(2\nu + 1)\pi/6$ where $\nu = 0, 1, 2$. $\nu = 3$ is equivalent to $\nu = 0$ repeating the pattern. This gives $k_W W = (2\nu + 1)\pi/6$ with $\nu = 0, 1$ and 2 for equivalent K or K' points, where k_W is the momentum vector along the width and k_L is along the length of the nanoribbon. The small width of GNRs can lead to quantum confinement of carriers that can be modeled analogous to the standing waves in a pipe open at both ends. The dispersion for a GNR is then given by

$$E = E_{F_0} \pm \hbar v_F |k| = E_{F_0} \pm \hbar v_F \sqrt{k_L^2 + \left((2\nu + 1) \frac{\pi}{6W} \right)^2} \quad (7)$$

This leads to bandgap equation

$$E = E_{F_0} \pm \frac{E_g}{2} \sqrt{1 + \left(\frac{3Wk_L}{\pi(2\nu + 1)} \right)^2} \quad (8)$$

In the parabolic approximation as for CNT, the bandgap and effective mass are given by

$$E_g = (2\nu + 1) \frac{\pi}{3W} \hbar v_F = (2\nu + 1) \frac{0.69 \text{ eV} \cdot \text{nm}}{W} \quad (9)$$

and

$$\frac{m_L^*}{m_o} = \nu \frac{\pi}{6W} \frac{\hbar}{v_F m_o} = (2\nu + 1) \frac{0.06 \text{ nm}}{W} \quad (10)$$

Fig. 6 gives the bandgap as a function of width with experimental values indicated that are spread between $\nu = 1$ and $\nu = 2$ configurations. The GNR bandgap and associated transport framework are sketchy as compared to that of a CNT.

3. CARRIER STATISTICS

The theoretical development of electronic transport in a graphene nanostructure is complicated due to linear E-k relation with zero effective mass of a Dirac fermion, as reviewed in a number of notable works [5-7]. An ideal graphene is a monoatomic layer of carbon atoms arranged in a honeycomb lattice. Monoatomic layer makes graphene a perfect two-dimensional (2D) material. As a 2D nanolayer, graphene sheet has some semblance to a metal-oxide-semiconductor field-effect-transistor (MOSFET). Wu et al [5]. give excellent comparison of linear E-k (energy versus momentum) relation in a graphene nanolayer to a quadratic one in a nano-MOSFET. Six-valley parabolic band structure in a MOSFET, even though anisotropic, has a finite effective mass [8-10]. As graphene is a relatively new material with a variety of its allotropes, the landscape of electronic structure and applications over the whole range of electric and magnetic fields is in its infancy [11].

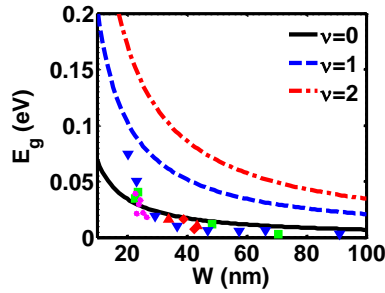


Fig. 6 The GNR bandgap as a function of width W . Markers are experimental data (M. Han et. al. *Phy. Rev. Lett.* 98, 206805(2007))

The Dirac cone described in Eq. (1) shows rise in energy with the magnitude of momentum vector:

$$E = E_{F_0} \pm \hbar v_F |k| = E_{F_0} \pm \hbar v_F \sqrt{k_x^2 + k_y^2} \quad (11)$$

where k is the momentum vector which in circular coordinates has components $k_x = k \cos \theta$ and $k_y = k \sin \theta$ and $v_F = (1/\hbar)dE/dk$ is constant due to linear rise of energy E with momentum vector k . $\hbar v_F$ is the gradient of E-k dispersion. The linear dispersion of Dirac cone is confirmed up to $\pm 0.6eV$ [3, 12]. $v_F \approx 10^6 m/s$ is the accepted value of Fermi velocity near the Fermi energy that lies at the cone apex $E_F - E_{F_0} = 0$ for intrinsic graphene with $E_{F_0} = 0$ as the reference level. The Fermi velocity vectors are randomly oriented in the graphene sheet.

The deviation $E_F - E_{F_0}$ of the Fermi energy from Dirac point defines the degeneracy of the Fermi energy that itself depends on 2D carrier concentration n_g as given by [4]

$$n_g = N_g \mathfrak{F}_1(\eta_c) \quad (12)$$

with

$$N_g = (2/\pi)(k_B T / \hbar v_F)^2 \quad (13)$$

$$\eta = (E_F - E_{F_0}) / k_B T \quad (14)$$

$\mathfrak{F}_j(\eta)$ is the Fermi-Dirac integral (FDI) of order j [13, 14] with $j=1$ for graphene.

The linear carrier density of CNT is similarly described by

$$n_{CNT} = N_{CNT} \mathfrak{F}_{CNT}(\eta, e_g) \quad (15)$$

with $e_g = E_g / k_B T$ and $N_{CNT} = D_0 k_B T$ the effective density of states with $D_0 = 4/\pi \hbar v_{F_0} = 1.93 \text{ eV}^{-1} \text{ nm}^{-1}$. $\mathfrak{F}_{CNT}(\eta, e_g)$ is the CNT integral that can be evaluated numerically [1]. Equilibrium carrier statistics for GNR is similarly obtainable.

In equilibrium, the velocity vectors are randomly oriented in the tubular direction with half oriented in the positive x-direction and half directed in the negative x-direction for a tubular direction along the x-axis. This makes the vector sum of velocity vectors equal to zero, as expected. However, the average magnitude of the carrier motion is not zero at a finite temperature. The group average velocity of a carrier in essence informs the speed of a propagating signal. It is also a useful parameter giving information as velocity vectors are re-aligned in the direction of an electric field [15] as it sets the limit at saturation velocity that is the ultimate attainable velocity in any conductor. In a ballistic transport when electrons are injected from the contacts, the Fermi velocity of the contacts plays a predominant role [16, 17]. It is often closely associated with the maximum frequency of the signal with which the information is transmitted by the drifting carriers. Formally, the carrier group velocity is defined as

$$v(E) = \frac{1}{\hbar} \left| \frac{dE}{dk} \right| \quad (16)$$

The magnitude of the velocity of Eq. (8.5.13) can be related to the DOS by rewriting it as

$$v(E) = \frac{1}{\hbar} \frac{dE}{dN} \frac{dN}{dk} = \frac{g_s}{2\pi \hbar D_{CNT}(E)} \quad (17)$$

where $\frac{dN}{dk} = \frac{g_s}{2\pi}$ (with $g_s = 2$ for spin degeneracy) in the k-space and $D_{CNT}(E) = dN / dE$ is the DOS for a single valley. When multiplied with the DOS and the Fermi-Dirac distribution function and divided by the electron concentration given by Eq. (3.9.15) the magnitude of the velocity vector, the intrinsic velocity v_i , for a CNT is given by

$$v_i = v_{F_0} \mathfrak{F}_0(\eta) / u_{CNT}, \quad u_{CNT} = n_{CNT} / N_{CNT} \quad (18)$$

The name intrinsic is given to this velocity as it is intrinsic to the sample as compared to the drift velocity that is driven by an external field. Similarly, the intrinsic velocity of GNR follows the same pattern $n_{GNR} = N_{GNR} \mathfrak{S}_{GNR}(\eta, e_g)$ as in Eq. (15).

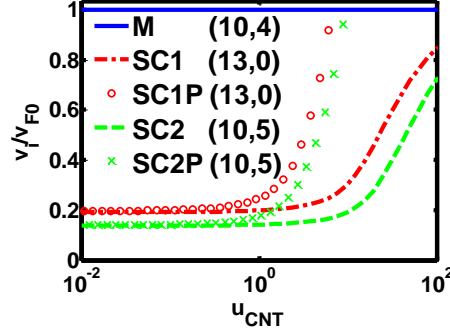


Fig. 7 The normalized intrinsic velocity v_i / v_{F0} as a function of normalized carrier concentration $u_{CNT} = n_{CNT} / N_{CNT}$ for different chiralities. P is parabolic approximation with effective mass

The intrinsic velocity and unidirectional velocity for arbitrary degeneracy are shown in Fig. 7 for band index $\nu = 0, 1, 2$. The intrinsic velocity is not equal to the Fermi velocity $v_{F0} \approx 10^6$ m/s for semiconducting samples approaching v_{F0} as expected in strong degeneracy. However, for a metallic CNT, the intrinsic velocity is the intrinsic Fermi velocity. The Fermi velocity in the parabolic model is calculable. However, it has no physical meaning as parabolic approximation works only in the nondegenerate regime.

The nonequilibrium carrier statistics is challenging considering a variety of approaches in the published literature with no convergence in sight. NEADF is natural extension of Fermi-Dirac statistics with electrochemical potential E_F during the free flight of a carrier changing by $q\vec{\mathcal{E}} \cdot \vec{\ell}$ where \mathcal{E} is the electric field and ℓ is the mean free path (mfp) [15]. NEADF is given by

$$f(E, \mathcal{E}, \theta) = \frac{1}{e^{\frac{E - (E_F - q\vec{\mathcal{E}} \cdot \vec{\ell})}{k_B T}} + 1} \quad (19)$$

NEADF is the key to transformation of stochastic velocity vectors into streamlined one giving intrinsic velocity that is the Fermi velocity in metallic state, but substantially below the Fermi level in semiconducting state. This intrinsic velocity v_i is lowered by the onset of a quantum emission. The nature of quantum (photon or phonon) depends on the substrate. A sample of intrinsic velocity in a CNT is given in Fig. 6. Intrinsic velocity is the average of the magnitude of the stochastic velocity with Fermi-Dirac distribution that is obtained from Eq. (19) when electric field is zero ($\mathcal{E} = 0$). This is the limit on the drift velocity as stochastic vectors in equilibrium transform to streamlined unidirectional vectors. In the metallic state, the saturation velocity is limited to v_{F0} . However, in a semiconducting state, it is substantially below v_{F0} . The parabolic (P) approximation, although simple in its appearance, is not valid in the degenerate realm.

Equal number of electrons has directed velocity moments in and opposite to the electric field ($n_+ = n_- = n/2$) in equilibrium, where n is the total concentration and n_{\pm}/n the fraction antiparallel (+) and parallel (-) to the applied electric field applied in the $-x$ -direction. The electron concentration $n_+ \gg n_-$ opposing electric field overpowers in the presence of an electric field as $n_{\pm}/n = \exp(\pm q\mathcal{E}\ell/k_B T)$. The fraction of electrons going in the $+x$ -direction (opposite to an applied electric field $\mathcal{E} = V/L$) is $\Delta n_+/n = \tanh(q\mathcal{E}\ell/k_B T)$. The drift velocity v_D as a function of electric field then naturally follows as [15]

$$v_D = v_u \tanh(q\mathcal{E}\ell/k_B T) \quad (20)$$

Here v_u is the unidirectional intrinsic velocity appropriate for twice the carrier concentration as electron cannot be accommodated in already filled state because of Pauli Exclusion Principle. In nondegenerate domain, the distinction between v_u and v_i is not necessary. The quantum emission can also be accommodated to obtain saturation velocity $v_{sat} = v_u \tanh(\Delta_Q/k_B T)$ that is smaller than v_u by quantum emission factor $\tanh(\Delta_Q/k_B T)$ approaching unity as energy of a quantum $\Delta_Q \gg k_B T$ goes substantially beyond the thermal energy. In the other extreme, when emitted quanta are much smaller in energy, the Bose-Einstein statistics limits $\Delta_Q/k_B T \approx 1$. Eq. (20) is strictly for nondegenerate statistics and that too for 1D nanostructures. Different expressions are obtained for 2D and 3D nanostructure. However, use of tanh function unifies the current-voltage profile that can be usefully employed for characterization in the wake of failure of Ohm's law. One way to preserve Eq. (20) for degenerate statistics is to define the degeneracy temperature T_e for electrons. The low field carrier drift velocity is obtained when $\Delta n_+/n$ is multiplied by v_{F_0} :

$$v_D = (\Delta n_+/n)v_{F_0} = \delta v_{F_0} [\mathfrak{I}_{-1}(\eta) / \mathfrak{I}_0(\eta)] \quad (21)$$

FDI approximates to $\mathfrak{I}_j(\eta) \approx \exp(\eta)$ for all values of j for nondegenerate statistics. The degenerate mobility expression is obtained from (11) by retaining the factor in bracket giving

$$\mu_o = q\ell v_{F_0} / k_B T_e \quad (22)$$

with

$$\frac{T_e}{T} = \frac{\mathfrak{I}_{-1/2}(\eta) v_{ud}}{\mathfrak{I}_{-3/2}(\eta) v_{id}} \quad (23)$$

where T_e is the degeneracy temperature signifying the higher energy of the degenerate electrons that is substantial higher than the thermal energy $k_B T$. Obviously $T_e/T = 1$ as expected. However, for strongly degenerate statistics $T_e/T = \eta$ giving $T_e = E_F/k_B$. The Fermi energy is $E_F = n_{CNT}/D_0$ for metallic degenerate CNT. T_e is therefore equal to $T_e = n_{CNT}/k_B D_0$.

4. I-V CHARACTERISTICS

In the graphene and CNT because of linear E-k relationship, the mobility expression is different from other semiconductors. A rudimentary analysis of the mobility in terms of mfp is to change mobility expression $\mu_{oo} = q\tau/m^* = q\ell_{oo}/m^*v$ by replacing $m^*v \rightarrow \hbar k =$

$(E_F - E_{F0})/v_F$. This gives a simple mobility expression that has been utilized in [4] in extracting mfp. The expression obtained from this analogy is

$$\mu_{\infty} = q\ell_{\infty}v_F / (E_F - E_{F0}) \quad (24)$$

The resistance then can be obtained from either $R_o = \rho_2 L / W$, with $\rho_2 = 1 / (n_2\mu_{on} + p_2\mu_{op})q$, for graphene with $n_2 \rightarrow n_g$ replacement for areal density for graphene and $n_1 \rightarrow n_{CNT}$ for CNT in $R_o = \rho_1 L$ $\rho_1 = 1 / (n_1\mu_{on} + p_1\mu_{op})q$. The velocity response to the high electric field is discussed in [4].

NEADF's transformation of equilibrium stochastic velocity vectors into a streamlined mode in extreme nonequilibrium leads to velocity saturation in a towering electric field. In a metallic CNT, the randomly oriented velocity vectors in equilibrium are of uniform Fermi velocity $v_{F0} = 1.0 \times 10^6$ m/s [1]. The saturation current $I_{sat} = n_{CNT}qv_{F0}$ arises naturally from this saturation, where $n_{CNT} = 1.53 \times 10^8$ m⁻¹ is the linear carrier concentration along the length of the tube consistent with experimentally observed [18] $I_{sat} = 21$ μ A. q is the electronic charge. The carrier statistics [1] gives $E_F = 67.5$ meV which is larger than the thermal energy for all temperatures considered (T = 4, 100, and 200 K), making applicable statistics strongly degenerate. The transition from ohmic to nonohmic saturated behavior initiates at the critical voltage $V_c = (k_B T / q\ell)L$ for nondegenerate statistics with energy $k_B T$ and $V_c = (E_F / q\ell)L$ for degenerate statistics with energy E_F . The mfp ℓ extracted from $R_o = 40$ k Ω is $\ell = 70$ nm that gives mobility [4] $\mu_o = q\ell v_F / E_F \approx 10,000$ cm² / Vs. The possibility of ballistic transport is miniscule given $\ell \ll L = 1$ μ m. The ballistic transport in 2D systems is extensively discussed by Arora and co-workers, [17, 19] where it is shown that the ballistic conduction degrades substantially the mobility in a 2D ballistic conductor with length smaller than the ballistic mfp. It may be tempting to apply the same formalism to 1D nanowire or nano CNT. However, the surge in resistance in a 1D resistor contradicts expected vanishing resistance for a ballistic conductor. A high-field resistance model [3] that employs the onset of phonon emission consistent with phonon-emission-limited mfp ℓ_Q of Tan et. al [20] explains very well the saturation in 2D GaAs/AlGaAs quantum well. Phonon-emission-limited mfp is generalized to any energy quantum by Arora, Tan, and Gupta [4]. ℓ_Q is the distance that a carrier travels before gaining enough energy $q\mathcal{E}\ell_Q = \Delta_Q$ to emit a quantum of energy Δ_Q with the probability of emission given by the Bose-Einstein statistics. $\ell_Q = \Delta_Q / q\mathcal{E}$ is infinite in equilibrium, very large in low electric field, and a limiting factor only in an extremely high electric field becoming comparable or smaller than the low-field mfp. That is why in the published literature on CNT, it is considered a high-field mfp, distinct from low-field scattering-limited mfp. It is ℓ_Q that was used by Yao et. al [18] to interpret the linear rise $R/R_o = 1 + (V/V_c)$ in resistance with the applied voltage. Here $R = V/I$ is the direct resistance. This direct resistance R cannot replicate the incremental signal resistance $r = dV/dI$. Therefore, the description of Yao et. al [18] is deficient in not employing the distribution function and hence does not attribute correctly the source of current saturation, the transition point to current saturation, and the paradigm leading to rise of direct and incremental resistance.

NEADF has a recipe for nonohmic transport leading to current saturation consistent with velocity saturation. As stated earlier, $n_+ \gg n_-$ in the presence of an electric field as $n_{\pm}/n = \exp(\pm q\mathcal{E}\ell/k_B T)$. The fraction of electrons going in the opposite direction to an applied electric field $\mathcal{E} = V/L$ is then $\Delta n_{\pm}/n = \tanh(q\mathcal{E}\ell/k_B T)$. The current-voltage relation with tanh function ($I = \Delta n_{\pm} q v_{F_0}$) is a derivative of rigorous degenerate statistics [15] with $V_c = (E_F/q\ell)L$ and magnitude of velocity vector equal to the Fermi velocity v_{F_0} for a metallic CNT. The current-voltage characteristics in a CNT are given by

$$I = I_{sat} \tanh(V/V_c) \quad (25)$$

Fig. 8 is a plot of Eq. (25) along with the experimental data of Yao et al [18]. Also shown are the lines at temperature $T = 4, 100,$ and 200 K following the rigorous degenerate statistics [15].

The distinction between direct $R = V/I$ and differential $r = dV/dI$ mode of resistance is crucial when I-V relation is nonlinear. R and r are given by

$$R/R_o = (V/V_c) / \tanh(V/V_c) \quad (26)$$

$$r/R_o = \cosh^2(V/V_c) \quad (27)$$

This relationship is in direct contrast to $R/R_o = 1 + (V/V_c)$ with $V_c = I_{sat}R_o$ used by Yao et. al [18], which can be obtained from Eq. (26) by using approximation $\tanh(x) \approx x/1+x$. I_o of Yao et. al is the same as I_{sat} .

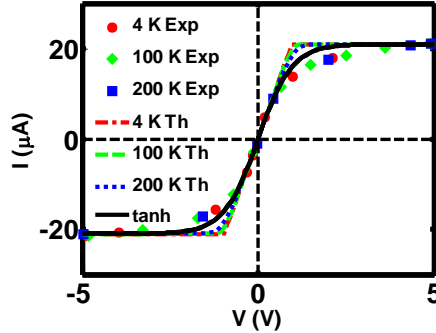


Fig. 8 I-V characteristics of a CNT of length $1 \mu m$. Th stands for theoretical curves derived from degenerate statistics. tanh curves are display of Eq. (25)

As shown in Fig. 9, the rise in r/R_o is exponential compared to linear rise in R/R_o . The potential divider rule between channel and contacts will make the lower-length resistor more resistive [21]. Hence great care is needed to ascertain the critical voltage V_c of the contact and channel regions.

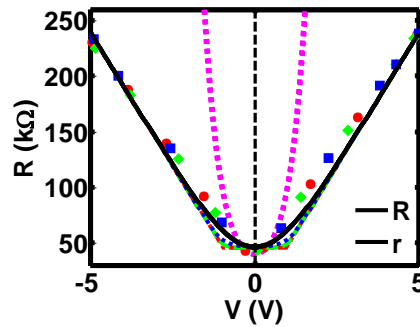


Fig. 9 R-V characteristics of a CNT of length $1 \mu m$. Markers and lines have same legend as in Fig.7. The differential resistance r (Eq. 27) rises sharply than the direct resistance R (Eq. 26)

Fig. 8 makes it clear that both direct slope I/V giving inverse resistance R^{-1} and incremental slope dV/dI giving differential (incremental) resistance r^{-1} decrease as voltage is increased ultimately reaching zero in the regime of saturation. However, in the work cited [4] the r is shown to decrease while conductance dV/dI increases with applied voltage. It may be noted that incremental resistance increases almost exponentially as indicated in Fig. 9 for $V > V_c$ and hence the curves are limited to a mV range to indicate superlinear surge of incremental resistance. Direct resistance does follow the linear rise with applied voltage.

The following observations are made consistent with the experimental data:

1. Ohmic transport is valid so far the applied voltage across the length of the channel is below its critical value ($V < V_c$).
2. The transition to nonlinear regime at the onset of critical electric field corresponding to energy gained in a mean free path is comparable to the thermal energy for nondegenerate statistics and Fermi energy for degenerate statistics [21, 22].
3. Resistance surge effect in ballistic channels corroborate well with that observed by Yao et. al [18] preceded by what was pointed out by Greenberg and Del Alamo[23] in 1994. The surge in contact region will change the distribution of voltage between contacts and the channel. In this light, Yao et. al [18] correctly conjectured that the measured resistance to be a combination of the resistance due to the contacts and the scattering-limited resistance of the CNT channel. The application of NEADF in CNT [1] gives not only the comprehensive overview of metallic and semiconducting band structure of CNT, but also elucidates the rise of resistance due to the limit imposed on the drift velocity by the Fermi velocity.
4. Onset of quantum emission lowers the saturation velocity. However, if quantum is larger than the thermal energy, its effect on transport is negligible [22]. It is important to employ Bose-Einstein statistics [4] to phase-in the possible presence of acoustic phonon emissions in addition to optical phonons or for that matter photons as transitions are induced by transfer to higher quantum level induced by an electric field. The phonon emission, generalized to quantum emission with Bose-Einstein statistics, is effective in lowering the saturation velocity only if the energy of the quantum is higher than the thermal energy. Quantum emission does not affect the ohmic mobility or for that matter ohmic resistance.

5. CONCLUSIONS

Carbon nano allotropes offer distinct advantage in meeting the expectations of *More than Moore* era. The paper reviews the complete landscape as graphene is rolled into a CNT or cut into a GNR. The rollover effect in terms of metallic (M) and semiconducting SC1 and SC2 is distinctly new given the competing explanation for chiral and achiral CNTs, making metallic CNT distinct from a semiconducting one. The same can be said of GNR where there is a complete absence of a semiconducting state. The NEADF is unique for high-field applications as it seamlessly makes a transition from ohmic domain to nonohmic domain. It is the nonohmic domain that is not interconnected in the published literature, necessitating the use of hot-electron temperature. NEADF clearly shows that hot-electron temperature is not necessary in description of high-field transport. The formalism presented connects very well the low-field and high-field regimes. The drive to reduce the size below the scattering-limited mfp is expected to eliminate scattering. This expectation goes against the experimental observation of rapid rise in the resistance [13, 21, 23-25]. This scattering-free ballistic transport, as is known in the literature, gives a resistance quantum $h / 2q^2 = 12.9 k\Omega$. However, if the length of CNT is larger than the scattering-limited mfp, the resistance will rise almost linearly. That is perhaps the reason that observed experimental resistance of $40.0 k\Omega$ as observed by Yao et. al [18] exceeds its ballistic value for a $1 - \mu\text{m}$ resistor. In fact, Greenberg and Del Alamo [23] have demonstrated that resistance surge in the parasitic regions degrades the performance of an InGaAs transistor. To sum it up, explorations of new physical phenomena on this length scale require the contributions from many different fields of science and engineering, including physics, chemistry, biology, materials science, and electrical engineering. However, quantum physics forms the backbone of understanding at a nanoscale in biochemical sciences where most applications of nanoensemble is apparent. This review exhibits new phenomena at the interface between the microscopic world of atoms and the macroscopic world of everyday experience that occur at the nanoscale. Such studies will undoubtedly lead to further applications with enormous benefit to society.

Acknowledgement: *The paper is a part of the research done at the Universiti Teknologi Malaysia (UTM) under the UTM Distinguished Visiting Professor program and UTM Research University Grant (GUP) Q.J130000.2623.04H32 of the Ministry of Education (MoE).*

REFERENCES

- [1] V. K. Arora and A. Bhattacharyya, "Cohesive Band Structure of Carbon Nanotubes for Applications in Quantum Transport," *Nanoscale* vol. 5, pp. 10927-10935, 2013.
- [2] A. K. Geim and K. S. Novoselov, "The rise of graphene," *Nature Materials*, vol. 6, pp. 183-191, Mar 2007.
- [3] P. H. S. Wong and D. Akinwande, *Carbon Nanotube and Graphene Device Physics*. Cambridge: Cambridge University Press, 2011.
- [4] V. K. Arora, M. L. P. Tan, and C. Gupta, "High-field transport in a graphene nanolayer," *Journal of Applied Physics*, vol. 112, p. 114330, 2012.
- [5] Y. H. Wu, T. Yu, and Z. X. Shen, "Two-dimensional carbon nanostructures: Fundamental properties, synthesis, characterization, and potential applications," *Journal of Applied Physics*, vol. 108, p. 071301, Oct 1 2010.
- [6] A. H. Castro Neto, F. Guinea, N. M. R. Peres, K. S. Novoselov, and A. K. Geim, "The electronic properties of graphene," *Reviews of Modern Physics*, vol. 81, pp. 109-162, Jan-Mar 2009.

- [7] K. S. Novoselov, S. V. Morozov, T. M. G. Mohiniddin, L. A. Ponomarenko, D. C. Elias, R. Yang, I. I. Barbolina, P. Blake, T. J. Booth, D. Jiang, J. Giesbers, E. W. Hill, and A. K. Geim, "Electronic properties of graphene," *Physica Status Solidi B-Basic Solid State Physics*, vol. 244, pp. 4106-4111, Nov 2007.
- [8] M. L. P. Tan, V. K. Arora, I. Saad, M. Taghi Ahmadi, and R. Ismail, "The drain velocity overshoot in an 80 nm metal-oxide-semiconductor field-effect transistor," *Journal of Applied Physics*, vol. 105, p. 074503, 2009.
- [9] I. Saad, M. L. P. Tan, A. C. E. Lee, R. Ismail, and V. K. Arora, "Scattering-limited and ballistic transport in a nano-CMOS circuit," *Microelectronics Journal*, vol. 40, pp. 581-583, Mar 2009.
- [10] V. K. Arora, M. L. P. Tan, I. Saad, and R. Ismail, "Ballistic quantum transport in a nanoscale metal-oxide-semiconductor field effect transistor," *Applied Physics Letters*, vol. 91, p. 103510, 2007.
- [11] V. E. Dorgan, M. H. Bae, and E. Pop, "Mobility and saturation velocity in graphene on SiO₂," *Applied Physics Letters*, vol. 97, p. 082112, Aug 2010.
- [12] I. Gierz, C. Riedl, U. Starke, C. R. Ast, and K. Kern, "Atomic Hole Doping of Graphene," *Nano Letters*, vol. 8, pp. 4603-4607, Dec 2008.
- [13] V. K. Arora and M. L. P. Tan, "High-Field Transport in Graphene and Carbon Nanotubes," presented at the International Conference on Electron Devices and Solid State Circuits 2013 (EDSSC2013), IEEEExplore Digital Library, Hong Kong Polytechnic University, 2013.
- [14] V. K. Arora, *Nanoelectronics: Quantum Engineering of Low-Dimensional Nanoensemble*. Wilkes-Barre, PA: Wilkes University, 2013.
- [15] V. K. Arora, D. C. Y. Chek, M. L. P. Tan, and A. M. Hashim, "Transition of equilibrium stochastic to unidirectional velocity vectors in a nanowire subjected to a towering electric field," *Journal of Applied Physics*, vol. 108, pp. 114314-8, 2010.
- [16] V. K. Arora, M. S. Z. Abidin, M. L. P. Tan, and M. A. Riyadi, "Temperature-dependent ballistic transport in a channel with length below the scattering-limited mean free path," *Journal of Applied Physics*, vol. 111, Mar 1 2012.
- [17] V. K. Arora, M. S. Z. Abidin, S. Tembhurne, and M. A. Riyadi, "Concentration dependence of drift and magnetoresistance ballistic mobility in a scaled-down metal-oxide semiconductor field-effect transistor," *Appl. Phys. Lett.*, vol. 99, p. 063106, 2011.
- [18] Z. Yao, C. L. Kane, and C. Dekker, "High-Field Electrical Transport in Single-Wall Carbon Nanotubes," *Physical Review Letters*, vol. 84, pp. 2941-2944, 2000.
- [19] V. K. Arora, "Ballistic Transport in Nanoscale Devices," presented at the MIXDES 2012 : 19th International Conference MIXED Design of Integrated Circuits and Systems, Wasaw, Poland, 2012.
- [20] L. S. Tan, S. J. Chua, and V. K. Arora, "Velocity-field characteristics of selectively doped GaAs/Al_xGa_{1-x}As quantum-well heterostructures," *Physical Review B*, vol. 47, pp. 13868-13871, 1993.
- [21] M. L. P. Tan, T. Saxena, and V. Arora, "Resistance blow-up effect in micro-circuit engineering," *Solid-State Electronics*, vol. 54, pp. 1617-1624, Dec 2010.
- [22] V. K. Arora, "Theory of Scattering-Limited and Ballistic Mobility and Saturation Velocity in Low-Dimensional Nanostructures," *Current Nanoscience*, vol. 5, pp. 227-231, May 2009.
- [23] D. R. Greenberg and J. A. d. Alamo, "Velocity saturation in the extrinsic device: a fundamental limit in HFET's," *IEEE Trans. Electron Devices*, vol. 41, pp. 1334-1339, 1994.
- [24] V. K. Arora, "Quantum Transport in Nanowires and Nanographene," presented at the 28th International Conference on Microelectronics (MIEL2012), Nis, Serbia, 2012.
- [25] T. Saxena, D. C. Y. Chek, M. L. P. Tan, and V. K. Arora, "Microcircuit Modeling and Simulation Beyond Ohm's Law," *IEEE Transactions on Education*, vol. 54, pp. 34-40, Feb 2011.